

Augmenting astrophysical scaling relations with machine learning: Application to reducing the Sunyaev-Zeldovich flux-mass scatter

Digvijay Wadekar^{a,b,1} 🗓, Leander Thiele^c, Francisco Villaescusa-Navarro^{de} 🗓, J. Colin Hill^{d,f} 🗓, Miles Cranmer^e 🗓, David N. Spergel^{d,e}, Nicholas Battaglia^g, Daniel Anglés-Alcázar^{d,h}, Lars Hernquistⁱ, and Shirley Ho^{d,e,j}

Edited by Daniela Calzetti, University of Massachusetts, Amherst, MA; received February 13, 2022; accepted December 7, 2022

Complex astrophysical systems often exhibit low-scatter relations between observable properties (e.g., luminosity, velocity dispersion, oscillation period). These scaling relations illuminate the underlying physics, and can provide observational tools for estimating masses and distances. Machine learning can provide a fast and systematic way to search for new scaling relations (or for simple extensions to existing relations) in abstract high-dimensional parameter spaces. We use a machine learning tool called symbolic regression (SR), which models patterns in a dataset in the form of analytic equations. We focus on the Sunyaev-Zeldovich flux—cluster mass relation $(Y_{SZ} - M)$, the scatter in which affects inference of cosmological parameters from cluster abundance data. Using SR on the data from the IllustrisTNG hydrodynamical simulation, we find a new proxy for cluster mass which combines Y_{SZ} and concentration of ionized gas $(c_{\rm gas})$: $M \propto Y_{\rm conc}^{3/5} \equiv Y_{\rm SZ}^{3/5} (1 - A c_{\rm gas})$. $Y_{\rm conc}$ reduces the scatter in the predicted M by $\sim 20 - 30\%$ for large clusters $(M \gtrsim 10^{14} \, h^{-1} \, M_{\odot})$, as compared to using just $Y_{\rm SZ}$. We show that the dependence on $c_{\rm gas}$ is linked to cores of clusters exhibiting larger scatter than their outskirts. Finally, we test Y_{conc} on clusters from CAMELS simulations and show that Y_{conc} is robust against variations in cosmology, subgrid physics, and cosmic variance. Our results and methodology can be useful for accurate multiwavelength cluster mass estimation from upcoming CMB and X-ray surveys like ACT, SO, eROSITA and CMB-S4.

cosmology | interpretable machine learning | hydrodynamic simulation

Astrophysical scaling relations are simple low-scatter relationships (generally power laws) between properties of astrophysical systems which hold over a wide range of parameter values. Such relationships have a large number of applications: i) inferring distances to objects, which is crucial for inferring cosmological parameters like the Hubble constant (H_0) see, e.g., the Leavitt period luminosity relation for Cepheids (1-3), Phillips relation for supernovae (4); ii) inferring properties of massive black holes e.g., the black hole-bulge mass/velocity dispersion relation (5–7); iii) inferring properties of galaxies e.g., the Tully Fisher relation (8) and its baryonic analog (9) for spiral galaxies, the Faber Jackson relation (10), the Kormendy relation or the more general fundamental plane relation (11–14) for ellipticals, the Color-Magnitude Relation; iv) providing insights into galaxy formation and evolution e.g., the stellar to halo mass relation (15); v) Inferring masses of galaxy clusters for cluster cosmology e.g., the Y-M relation (16–18), $M_{\rm gas}-M$ relation (19, 20), Mass-richness relation (21). Note that many of these relations have been discovered phenomenologically—often by trial and error—from observational data/simulations, rather than being derived from first principles*.

Most of the scaling relations found in astrophysics till now are power-law relations which involve only two variables. A reason for this could just be that it is easy to visually identify two-parameter relations in a dataset. There could exist many low-scatter relations with three or more variables in existing data which have been overlooked as it can be tedious to identify such relations with manual data analysis. For instance, some of the popular two-parameter relationships were later shown to extend to three dimensions only by a more detailed subsequent analysis, e.g., the fundamental plane relationship for elliptical galaxies. One of the traditional approaches to identify a high-dimensional nonlinear hypersurface in a dataset is by looking at various 2D projection plots.

Significance

Two-dimensional power-law relationships discovered empirically in observed or simulated data are used for inferring properties of a wide variety of astrophysical objects (e.g., stars, supernovae, and galaxies). More accurate relations, which are nonlinear, or contain three or more variables, could easily have been overlooked, as they are difficult to find with manual data-analysis methods. We show that machine learning tools can expeditiously search for such relations in high-dimensional astrophysical data-spaces. In particular, we find improvements to previous relations which have been widely used for estimating masses of clusters of galaxies. Numerous upcoming observational surveys will target galaxy clusters, and our work enables their use to more accurately infer the fundamental properties of the Universe.

Author contributions: D.W., F.V.-N., J.C.H., D.N.S., N.B., L.H., and S.H. designed research; D.W. and L.T. performed research; D.W., L.T., F.V.-N., M.C., D.A.-A., and L.H. contributed new reagents/analytic tools; D.W. and L.T. analyzed data; and D.W. wrote the paper.

The authors declare no competing interest.

This article is a PNAS Direct Submission.

Copyright © 2023 the Author(s). Published by PNAS. This article is distributed under Creative Commons Attribution-NonCommercial-NoDerivatives License 4.0

¹To whom correspondence may be addressed. E-mail:

This article contains supporting information online at http://www.pnas.org/lookup/suppl/doi:10.1073/pnas. 2202074120/-/DCSupplemental.

Published March 17, 2023

^{*}It is interesting to mention that, in some areas of physics, discovery of empirical relations has sometimes led to deep theoretical insights—take Kepler's laws giving inspiration to Newtonian mechanics, or the Planck equation (also an empirical function fit) aiding the development of Quantum Mechanics.

This approach, however, becomes increasingly difficult and time consuming with larger datasets.

Machine learning (ML) tools can provide a faster and a more systematic approach to search for nonlinear low-scatter relationships in abstract high-dimensional parameter spaces. ML tools are increasingly useful as datasets available in astrophysics continue to grow in size due to advent of high-precision multiwavelength surveys. A particularly useful ML tool to search for new scaling relations, or to find extensions to existing ones, is symbolic regression (SR). SR identifies equations with parsimonious combinations of input parameters that have the smallest scatter with the given quantity of interest.

SR, also known as automated equation discovery, has been studied for decades in the context of scientific discovery, including early work creating the "BACON" algorithm (22) and its later implementations including COPER (23) and FAHRENHEIT/EF (24, 25). More recent work by refs. 26 and 27 popularized SR for science and introduced the software package Eureqa, which is a powerful (but proprietary) library still in use today. This preceded significant interest from the ML community in advancing fundamental search techniques, including (28-42). In parallel, these algorithms have been applied to a range of scientific problems, such as (39, 43-57). It is worth mentioning that SR has been used in various astrophysical applications: modeling assembly bias (43, 44); estimating photometric redshifts of galaxies (57); inferring universal subhalo properties (47); modeling the concentration of dark matter from the mass distribution of nearby cosmic structures (39); discovering relationships in time-domain astronomy (45, 46); finding analytic forms of the one-point probability distribution function for neutrino-density fluctuations (58); and modeling the SFR density as a function of cosmological and astrophysical feedback parameters (59).

In order to put SR in context, we illustrate tradeoffs in available ML tools along various dimensions in Fig. 1. Deep learning tools like neural networks can handle very high-dimensional inputs and large datasets but are the least interpretable. SR lies on the opposite side of this spectrum: as of today, SR can be applied to datasets with only \lesssim 10,000 data points, each with \lesssim 10 parameters. One must therefore simplify the problem or at times subsample the data in order to use SR on it. We follow the approach of ref. 44, where we first reduce the dimensionality of our dataset using a decision-tree-based approach called a random forest regressor and then apply SR on it. Using the minimum set of relevant variables as input to SR is important to speed up its search for optimal equations.

We will focus on applying SR to find accurate expressions that relate properties of galaxy clusters to their masses. Galaxy clusters are the most massive bound structures in the Universe and their abundance as a function of mass is a very sensitive probe of cosmology (16, 60-66). In the 2020s, many ongoing and upcoming surveys (e.g., Rubin observatory, DES, HSC, DESI, ACT, eROSITA, SO, CMB-S4) will provide a wealth of multiwavelength data on clusters. If we can obtain robust mass estimates for these clusters from this data, we will be able to put very strong constraints on the nature of dark energy and neutrino masses (67-72). Cluster masses are typically inferred from properties easily measurable in observational surveys. For example, CMB surveys use the integrated electron pressure (Y_{SZ}) via the mass-observable power-law relationship † : $M_{\rm cluster} \propto Y_{\rm SZ}^{3/5}$ (the observable properties thus used are referred to as 'mass

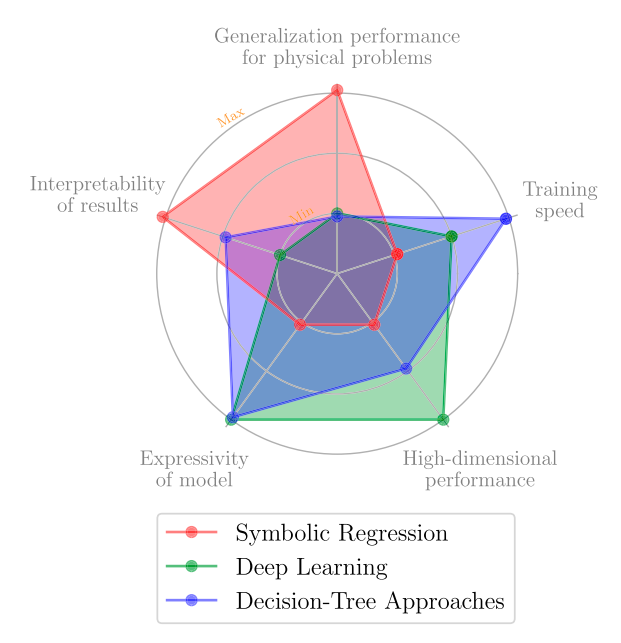


Fig. 1. Various aspects of the trade-offs between machine learning (ML) techniques. Symbolic regression can robustly be applied to datasets with only \lesssim 10,000 data points, each with \lesssim 10 parameters. On the other hand, it can provide analytic equations that are readily interpretable and generalizable. We first use a decision-tree-based approach called random forest regressor to narrow down the set of parameters that impact the scatter in the Y-M relation. We then implement symbolic regression to find an analytic form for a cluster mass proxy using the preselected parameters.

proxies'). The scatter in these relationships affects the accuracy to which the masses—and thereby the cosmological parameters can be inferred (73) (e.g., the uncertainty in the scatter can be a source of systematic bias). Therefore, an important property of a mass proxy is that the scatter in its relation with mass should be well-characterized and small.

A combination of observable properties (sometimes measured in different surveys) could sometimes provide a lower scatter mass proxy. For example, X-ray studies show that the product of gas mass, $M_{\rm gas}$, and gas temperature, T_X , provides a lower scatter proxy than X-ray luminosity, gas mass, or temperature: $Y_X \equiv M_{\rm gas} T_X (17)^{\ddagger}$. Recently, it has become possible to measure numerous properties of clusters: cluster electron pressure with SZ surveys, gas density, and temperature profiles with X-ray surveys, density profiles with weak lensing surveys, spectra and color of galaxies in optical surveys, and diffuse synchrotron flux in radio surveys. In order to construct an optimal mass proxy from these, one encounters the following challenges: i) Which particular properties in this large set to combine together? ii) What functional form should be used to fit the combination?

ML methods can be useful for such problems. It is worth mentioning that there have been many recent ML-motivated approaches to estimate cluster masses: (39, 78-93). Our goal in this paper is to model M_{cluster} by approximating the following function

$$M_{\text{cluster}} = f(Y_{\text{SZ}}^{3/5}, \{i_{\text{obs}}\}),$$
 [1]

with ML tools like random forests and symbolic regressors. $\{i_{obs}\}$ is the set of various observable properties from multiwavelength cluster surveys (e.g., gas mass, gas profile, richness, and galaxy colors). As clusters are nonlinear objects, there are no obvious

 $^{^\}dagger$ In practice, the power-law exponent is calibrated with observational data; however, the actual fitted values are fairly close to 3/5, which is the prediction from virial theorem.

[‡]There have also been similar studies on augmenting the Y - M relation (74–77); we will discuss them later in section 5C.

first principles predictions for which properties in $\{i_{obs}\}$ should contribute. Furthermore, the high dimensionality of $\{i_{obs}\}$ makes this a complex and challenging problem for traditional methods.

The paper is organized as follows. In *Cluster Data and Properties*, we briefly describe the cluster data that we use from various hydrodynamical simulations. In *Mass Proxies*, we present an overview of mass proxies. We then discuss an overview of our ML techniques in *Machine Learning Techniques* and show the results for cluster mass prediction in *Results for Y-M Scatter*. We describe our reasoning behind using cluster concentration in *Discussion*, and we conclude in *Conclusions*.

1. Cluster Data and Properties

In this section, we provide a brief description of the cluster data that we employ in our analysis. We use the TNG300-1 simulation (hereafter TNG300) produced by the IllustrisTNG collaboration $(94-101)^{\S}$, which is run with the moving mesh AREPO code (102, 103). We use the cluster samples from two different snapshots at redshifts $z = \{0, 0.7\}$ in our study.

We also use clusters from the CAMELS suite of simulations (59, 104), which consists of more than 2,000 hydrodynamic simulations (each simulation box has length 25 $h^{-1} Mpc$) run with different baryonic feedback and cosmological parameters, and with varying initial random seeds. CAMELS contain two distinct simulation suites, depending on the code used to solve the hydrodynamic equations and the subgrid model implemented: i) CAMELS-SIMBA, based on the GIZMO code (105, 106) employing the same subgrid model as the flagship SIMBA simulation (107); ii) CAMELS-TNG, based on the AREPO code employing the same subgrid model as the flagship IllustrisTNG simulations. Let us provide one example to highlight the substantial differences in these models: Feedback from active galactic nuclei (AGN) is implemented considering Bondi accretion and spherical symmetry in IllustrisTNG (108), while SIMBA implements gravitational torque accretion of cold gas and collimated outflows and jets from AGN (109). We use clusters in the z = 0 snapshots of the Latin hypercube set for our analysis. (See ref. 59 for further details on the CAMELS simulations.)

For all the simulations, we work with halos identified by the FOF friends-of-friends, also referred to as single linkage hierarchical clustering (110) algorithm with linking length 0.2. We choose the centers of clusters to be the locations of the minimum gravitational potential within the FOF volume. Note however that, to calculate properties of clusters mentioned later in this section, we do not use the FOF volume but instead use the spherical definition of clusters (we refer the reader to ref. 111 for the advantages of using a spherical halo definition over the FOF volume). We use the boundary R_{200c} to define the cluster radii[#]. M_{200c} is the mass of all the particles (dark matter, gas, stars, and black holes) within R_{200c} of the center of the halo. Note that we will use the 3D data of clusters in this paper; in reality, however, projected properties, instead of 3D, are measured in surveys; we will test our results for that case in a future study. We show the number of clusters as a function of their masses in SI Appendix Fig. S1. Let us now discuss the cluster properties we use in our study.

(i) Integrated electron pressure: CMB photons are scattered by high-energy electrons in the plasma inside clusters due to inverse

Compton scattering. This phenomenon is known as the thermal Sunyaev-Zeldovich (tSZ) effect and it induces a shift in the energy of the scattered CMB photons (112). Such a shift is typically parameterized by the integrated Compton-y parameter (Y_{SZ}) and can be directly measured in SZ surveys. We measure a 3D analog of it in simulations, as given by,

$$Y_{200c} = \frac{\sigma_{\rm T}}{m_e c^2} \int_0^{R_{200c}} P_e(r) \, 4\pi \, r^2 dr, \qquad [2]$$

where σ_T is the Thomson cross-section, m_e is the electron mass, P_e is the electron pressure, and c is the speed of light. Note that we use the group_particles code to obtain $P_e(r)$ (and most other properties mentioned in this section) from the simulation data. (ii) Ionized gas mass: We calculate the cluster ionized gas mass $(M_{\rm gas})$ as,

$$M_{\rm gas}(r < R) = \frac{2}{1 + X_H} m_p \int_0^R n_{\rm e}(r) \, 4\pi \, r^2 dr,$$
 [3]

where n_e is the free electron number density profile, $X_H = 0.76$ is the primordial neutral hydrogen fraction, and m_p is the proton mass. Note that we derive $M_{\rm gas}$ from the electron density profile of a cluster in order to mimic the $M_{\rm gas}$ measurements from X-ray surveys where $n_{\rm e}(r)$ is derived by deprojecting of X-ray surface brightness profiles (20, 113).

(iii) Cluster concentration: We use different versions of the cluster concentration in this paper. For the main results, we use concentration corresponding to the gas profile: $c_{\rm gas} \equiv M_{\rm gas}(r < R_{200c}/2)/M_{\rm gas}(r < R_{200c})$. We also perform additional cross-checks using the concentration obtained by fitting an NFW profile to the halos. In particular, we use $c_{\rm NFW} \equiv R_{\rm vir}/R_{\rm scale}$ ($R_{\rm vir}$ is the virial radius and $R_{\rm scale}$ is the Klypin scale radius (114) corresponding to the largest subhalo in the halo) measurements by ref. 115, which were obtained by running the Rockstar code (116) on the TNG300 halos.

(iv) Stellar mass: We calculate M_* by summing over of the masses of all the star particles within R_{200c} . Note that this quantity represents thus the total stellar mass in the cluster, not the stellar mass of the central galaxy.

(v) Cluster triaxiality: We generally expect clusters to be triaxial since they are formed by accretion along filaments that can impose a tidal gravitational force upon the forming clusters. We first calculate the moment of inertia tensor using,

$$T_{ij} \equiv \sum_{\alpha} m_{\alpha} (x_{i,\alpha} - \bar{x}_i)(x_{j,\alpha} - \bar{x}_j),$$
 [4]

where \bar{x}_i is the coordinate of the center-of-mass of the cluster and m_{α} is the particle mass (we only use the particles within R_{200c} of the cluster center in our calculations). We calculate T_{ij} in two different ways: first, using all particle types (gas+stars+DM+black holes); second, using only the gas particles. We then calculate the triaxiality of the cluster as λ_1/λ_3 where λ_i are eigenvalues of T_{ij} ordered as $\lambda_1 < \lambda_2 < \lambda_3$. We also check our results with a different definition of triaxiality: $(\lambda_1 - \lambda_3)/2/(\lambda_1 + \lambda_2 + \lambda_3)$. (vi) Cluster richness: The richness of a cluster is the number of galaxies associated with it. We select the galaxies using the threshold $M_{\star} > 10^9 \ h^{-1} M_{\odot}$ and by requiring the centers of the galaxies to be within R_{200c} of the cluster center. At z=0, this threshold yields a number density of galaxies in the simulation sample of $\sim 0.02 \ (h/{\rm Mpc})^3$.

[§]IllustrisTNG: https://www.tng-project.org/data/.

[¶]CAMELS: https://camels.readthedocs.io.

 $^{^{\#}}R_{200c}$ is the radius enclosing an overdensity $\Delta=200$ with respect to the critical density of the Universe.

https://github.com/leanderthiele/group_particles.

2. Mass Proxies

Simple models of clusters based on the virial theorem (which assumes that the only source of energy input into the intracluster medium is gravitational) predict nearly self-similar relations between halo mass and various dynamic properties (117, 118). For example, the scaling relation between cluster masses and temperature is given by ref. 119:

$$T \propto (M E(z))^{2/3},$$
 [5]

where $E(z) \equiv H(z)/H_0 = \sqrt{\Omega_m(1+z)^3 + \Omega_\Lambda}$ for a flat Universe. Note that the temperature also depends on the value of Δ (the overdensity with respect to the critical density of the Universe used for defining the cluster boundary); we have absorbed this dependence under the proportionality sign. The scaling relation for the gas mass of a cluster is simply $M_{\rm gas} \propto M$. Using Eqs. 2 and 5, one can write a scaling relation for the integrated Compton— γ parameter given by,

$$Y_{\rm SZ} \propto M_{\rm gas} T \propto M^{5/3} E(z)^{2/3}$$
. [6]

Scaling relations like these help in determining various possible proxies of cluster mass, e.g.,

$$M \propto Y_{\rm SZ}^{3/5} E(z)^{-2/5}$$
. [7]

In addition to being motivated by idealized scaling relations, a mass proxy should have additional properties: i) Robustness: it should be largely insensitive to limitations in our understanding of clusters, baryonic feedback effects, or their merger history, ii) Accuracy: it should have a small and well-characterized scatter in the relation with mass, and iii) Low cost: it should be observationally inexpensive in order to be applied for mass prediction of thousands of clusters.

 $Y_{\rm SZ}$ satisfies all the aforementioned requirements. The self-similar evolution of the $Y_{\rm SZ}$ -M relation for clusters is also remarkably insensitive to baryonic physics like AGN feedback or radiative cooling (18, 120–122). The $Y_{\rm SZ}$ -M relation can be calibrated using two types of gravitational lensing measurements: CMB lensing measurements (which offer the advantage of a very well-determined distance to the source plane) (123–126) and optical weak lensing surveys (which provide higher S/N measurements for individual clusters) (127–132). Analogs of $Y_{\rm SZ}$ have therefore been used for cluster mass estimation in CMB surveys like Planck (16, 60, 61), ACT (62, 63), and SPT (64, 65). It is worth mentioning that there are also proposals to self-calibrate the relation (133, 134). An analog of $Y_{\rm SZ}$ called $Y_{\rm X}$ is also used in X-ray surveys for mass estimation (17, 121). For a comprehensive review of the $Y_{\rm SZ}$ -M relation, see ref. 18.

We show the $Y_{200c} - M_{200c}$ relation from Eq. 7 for TNG300 clusters in Fig. 2 (Eq. **2** for the definition of Y_{200c}). For comparison, we also show the performance of other mass proxies like $M_{\rm gas}$ and cluster richness in *SI Appendix*, Fig. S2. For a large region of parameter space in Fig. 2, the clusters closely follow the self-similar scaling relation** with low scatter. Reducing the scatter further is imperative as the uncertainty in the mass-observable relation is currently the largest systematic uncertainty in cosmological analyses of galaxy clusters.

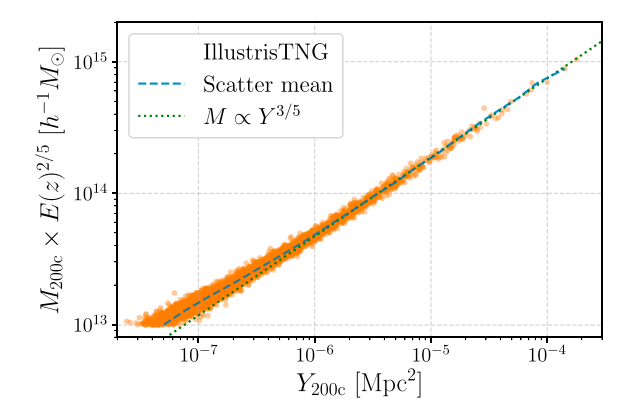


Fig. 2. *Y-M* scaling relation in clusters from the TNG300 simulation at $z = \{0, 0.7\}$ (Y_{200c} [M_{200c}] is the integrated Compton-y parameter [cluster mass] within R_{200c}). The self-similar power-law scaling relation normalized to the most massive halos is shown by the dotted green line. The goal of this paper is to improve this scaling relation in order to reduce its scatter and infer cluster masses more accurately.

As we can see from Fig. 2, $M_{\rm cluster} \propto Y_{\rm SZ}^{3/5}$ is a very good first approximation; we therefore train our ML models to approximate the following function based on the residuals:

$$M_{200c}/Y_{200c}^{3/5} = g(\{i_{\text{obs}}\}).$$
 [8]

In this way, we incorporate the domain knowledge (in our case the already well-established leading-order cluster physics) and use ML only to learn extensions to it.

3. Machine Learning Techniques

We now continue our discussion of machine learning (ML) techniques from the introduction section. In Fig. 1, we had compared the ML techniques along two particular dimensions. Deep neural networks (DNNs) are on one extreme: they can work with very high-dimensional datasets or datasets with large sizes. There also have been many interesting applications of DNNs to cosmology (see, e.g., refs. 39, 54, 141–161). However, DNNs are notoriously difficult to interpret due to the high-dimensional parameter space of the model (typically $\gtrsim 10^6$ parameters). Furthermore, DNNs typically require very large datasets to train, whereas in our case, we only have ~200 clusters with $M_{200c} > 10^{14} \, h^{-1} \, M_{\odot}$ in the TNG300 sample. We therefore used the two techniques detailed below, both of which can have better performance than DNNs on small datasets.

A. Random Forest. A random forest regressor (RF) is a collection of decision trees; each tree is in itself a regression model and is trained on a different random subset of the training data (162) (random forests can also be used for classification tasks, but here we use them for regression). The output from a RF is the mean of the predictions from the individual trees (a single decision tree is prone to overfitting and using the ensemble mean of different trees reduces overfitting) (163). RFs have been used for various applications in astrophysics: (78, 79, 164–172). As they allow one to easily infer the relative importance of each input feature, they are slightly better suited with regard to interpretability as compared to deep neural networks. Other advantages of decision tree-based algorithms are that they are comparatively much faster to train and they do not require access to GPUs.

^{**}A perceptive reader would notice that there is a deviation/break from the power-law relation in Fig. 2 for low-mass clusters. This is because gas in the cluster gets ejected at low masses since the gravitational potential wells are comparatively shallower (135–139). We only focus on high mass clusters in this paper as only those are typically used in cosmological analyses; we have however modeled the deviations from self-similarity in a more recent paper (140).

We use RF from the publicly available package Scikit-Learn^{††} (173). In order to check whether the results from the RF are robust to overfitting, we divide the data into two categories: We use a subsample containing $\sim 40\%$ of the clusters to train the RF, and the rest are used in testing the RF. We show the results from the test set later in *Results for Y-M Scatter A*. Note that we do not use RF for the final results of this paper, but only as a feature selection tool for making the application of symbolic regression easier.

B. Symbolic Regression. Symbolic regression (SR) is a technique that approximates the relation between an input and an output through analytic mathematical formulae. The difference between using it versus ordinary "least squares" regression is that knowledge of the underlying functional form of the fitting function is not required a priori. The advantage of using SR over other machine learning regression models is that it provides analytic expressions which can be readily generalized and also facilitates the understanding of the underlying physics. One of the downsides of SR, however, is that the dimensionality of the input space needs to be relatively small. To overcome this, we first use the RF to obtain an indication of which parameters in the set of $\{i_h\}$ in Eq. 8 give the most accurate M_{200c} . We then compress the $\{i_h\}$ set to include only the five most important parameters. Finally, we use SR on the compressed set to obtain an explicit functional form to approximate f from Eq. 8. We use the symbolic regressor based on genetic programming implemented in the publicly available PvSR package^{‡‡} (39, 40).

Let us briefly describe the procedure to fit a function with the PySR package. First, we specify the relevant input parameters (in our case, $\{c_{\text{gas}}, M_{\text{gas}}, M_*, c_{\text{NFW}}\}$). We also need to specify unary and binary operators as input; we have chosen: binary operators= [sum (+), multiplication(·), division(/), power], and unary operators = [negative, exponential, absolute value]. Using genetic programming, the SR then generates multiple iterations of formulae (e.g., $2.7 \cdot M_*^2 + \exp(M_{\text{gas}}/c_{\text{gas}})$). The best equations are decided based on their complexity and the specified loss function (equations which are the simplest and simultaneously give the least loss are preferable).

We use an analog of the L1 loss function, given by,

Loss =
$$\sum_{i \in \text{clusters}} w_i | M_i^{\text{true}} - M_i^{\text{predicted}} |$$
. [9]

The reason for choosing the L1 loss instead of L2 (i.e., Loss $\propto |\Delta M|^2$) is that it is as it is more robust to cases when the scatter is large. In other words, it is less susceptible toward outliers (see also other robust loss functions like Huber loss). As the number of halos decreases with their mass, we use the weights $w_i = M_i^{1/2}$ to upweight the high-mass halos (the weights also help in accounting for increased scatter towards low masses). Our primary focus in this paper is on clusters with $M \gtrsim 10^{14} \ h^{-1} \ M_{\odot}$ as lower mass clusters are not used for probing cosmology (the lower mass regime is relatively more affected by AGN/supernova feedback). We specifically focus on improving Y-M relation for low-mass regime in a more recent paper (140). As separation between most clusters is too large for them to affect each other's evolution, we assume that their mass residuals are independent in the loss function in Eq. 9.

The complexity penalty of equations from SR is determined by the number of operators, free constants, and variables in them. We use the default setting of equal complexity of individual operators, constants, variables (one also has the option to specify different values of complexity penalty to different operators, e.g., sin can be set to have three times the penalty of +). Note that there are traditional criteria to evaluate complexity of different fitting functions, e.g., Bayesian Information Criterion (BIC) or Akaike Information Criterion (AIC). However, such criteria typically only penalize the number of free constants and do not take into account the number of operators or variables in the equations, making them difficult to apply directly to output equations from SR.

It is worth mentioning that instead of needing to explicitly specify a parametric form like Eq. **9** for the loss function, there are various nonparametric methods for fitting relations to data. A few examples are quantile regression and local regression models (e.g., Gaussian processes, local polynomial models like LOWESS) (173–176). Such methods are relatively advantageous to use when errors are heteroscedastic (i.e., the scatter is nonuniform, which is also the case for Y-M relation at low masses) or the data contain outliers. These methods have been used in various astrophysical applications, e.g., refs. 177, 178, and 179. However, we do not use them in our work as current SR packages require a parametric form of loss function to be specified (to our best knowledge, they are not currently designed to work with nonparametric loss functions).

4. Results for Y-M Scatter

In this section, we compare the results from ML methods against the standard Y-M relation. Most of the studies which carry out the analysis of Y-M for cluster cosmology assume that the scatter is log-normal (62, 63, 65) see however (18, 77). We therefore choose to compare the performance of different mass estimation methods using the following statistic:

$$\sigma_i \equiv \left[\frac{1}{N_i} \sum_{j}^{N_i} (\log M_j^{\text{true}} - \log M_j^{\text{predicted}})^2\right]^{1/2}, \quad [10]$$

where *i* corresponds to individual mass bins containing N_i clusters (we used uniformly spaced bins in log-space).

A. Results from the Random Forest. We train the RF regressor using various cluster properties from *Cluster Data and Properties* and show results in Fig. 3. In the bottom panel, we use Eq. **10** to calculate the scatter and show the relative improvement in the mass prediction (the improvement is $\gtrsim 30\%$ for the best-case scenario). We do not compare the scatter for the very high-mass end as there are very few halos available to calculate the scatter robustly.

We also used cluster richness and triaxiality as input to the RF but did not notice any improvement in our results; we therefore do not show lines corresponding to them in Fig. 3. We show the feature importance assigned by the RF to various input variables in *SI Appendix* Fig. S3. We also tried using other galaxy properties (e.g., color of the brightest cluster galaxy), but we did not find any improvement in the scatter prediction.

B. Symbolic Regression. Using the RF, we identified that the parameters $c_{\rm gas}$, $M_*/M_{\rm gas}$ and $c_{\rm NFW}$ have the largest effect on the mass prediction. We now train the symbolic regressor to model the function in Eq. **8** using these properties and obtain

^{††}Random forest: https://scikit-learn.org/stable/modules/generated/sklearn.ensemble.

^{‡‡}PySR: https://github.com/MilesCranmer/PySR.

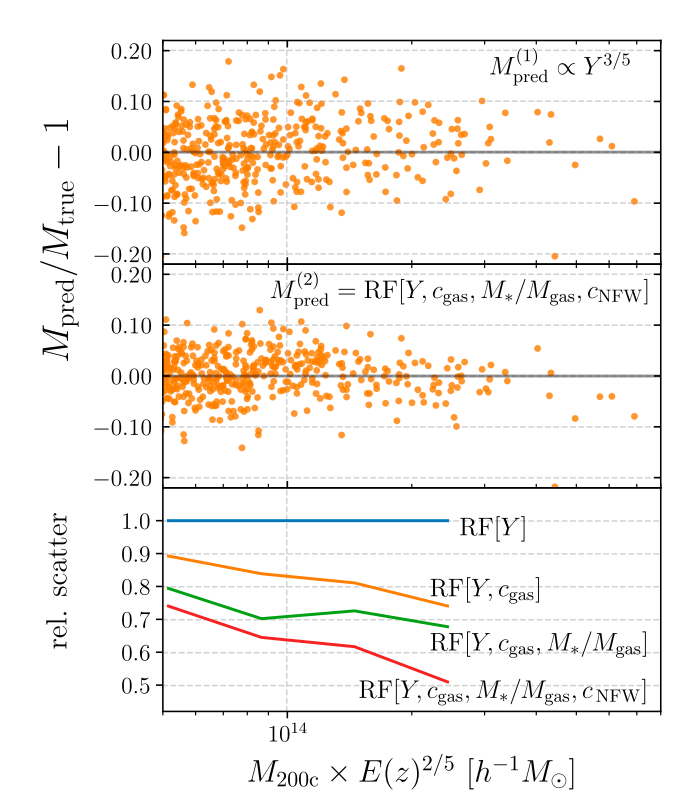


Fig. 3. Results from prediction of cluster masses with a random forest regressor (RF). Scatter in the predicted mass using the traditional Y-M relation (RF) is in *Top (Middle)* panel. The *Bottom* panel shows the effect of different sets of input parameters on the mass prediction. $c_{\rm gas}$ is the concentration of gas from Eq. **12**, $c_{\rm NFW}$ is the NFW concentration, M_* ($M_{\rm gas}$) is the stellar (gas) mass within $R_{\rm 200c}$. Overall, the RF improves mass prediction by \gtrsim 30% as compared to the traditional scaling relation method.

the results shown in Fig. 4. Our main result of the paper is the following mass proxy which improves the cluster mass prediction as compared to using the standard Y-M relation:

$$M \propto Y_{\rm conc}^{3/5} \equiv Y_{200c}^{3/5} \left[1 - A c_{\rm gas} \right],$$
 [11]

where c_{gas} is related to the concentration of the halo gas profile and is given by,

$$c_{\rm gas} \equiv \frac{M_{\rm gas}(r < R_{200c}/2)}{M_{\rm gas}(r < R_{200c})},$$
 [12]

where $M_{\rm gas}(r)$ is given by Eq. 3 and can be estimated from X-ray surveys. A is a dimensionless parameter and we obtain the best-fit value A=0.4 for the TNG300 sample (we generally expect $A \in [0,1]$). We will discuss the physical explanation behind the better performance of $Y_{\rm conc}$ in Section 5.

We also found that replacing c_{gas} in Eq. 11 by an analogous parameter:

$$c_Y \equiv \frac{Y(r < R_{200c}/2)}{Y(r < R_{200c})},$$
 [13]

gives a very similar improvement in the mass prediction. The advantage of using c_Y over $c_{\rm gas}$ is that one does not need X-ray observations of clusters and SZ measurements alone are sufficient. On the other hand, it may not be straightforward to resolve scales of $R_{200c}/2$ (i.e., $\sim 0.7 R_{500c}$) in the observations of clusters from upcoming SZ surveys like SO and CMB-S4 due to their low resolution. §§

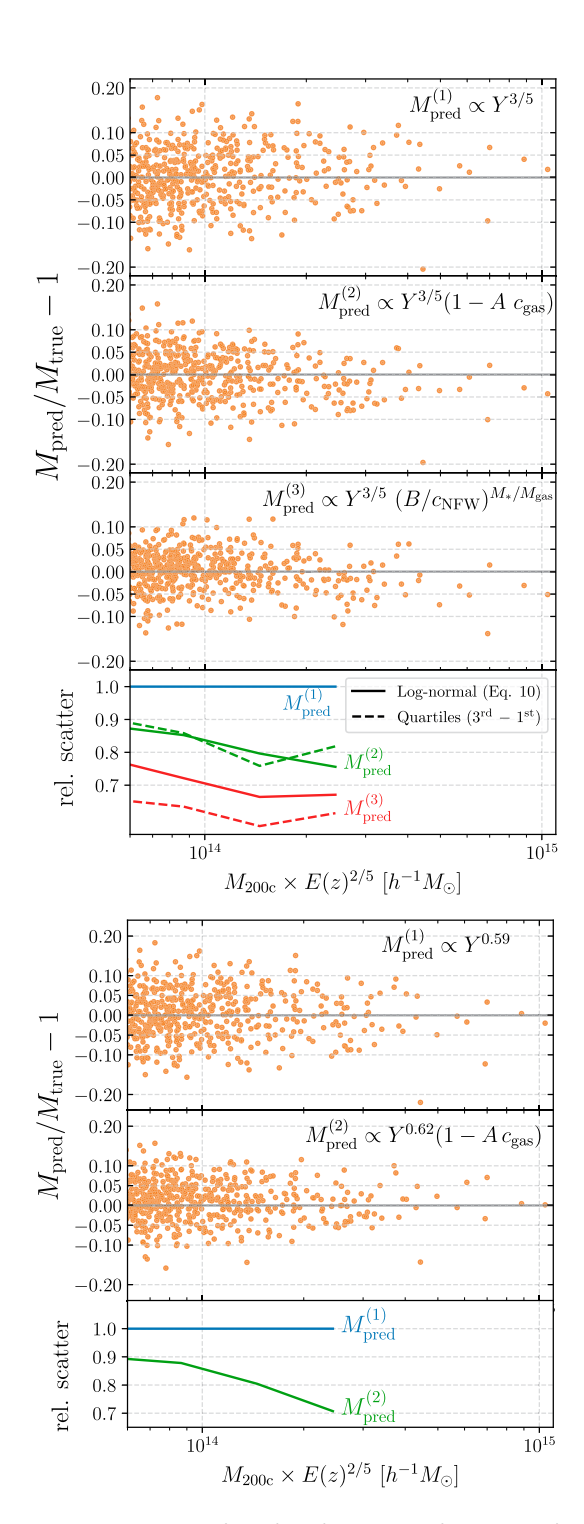


Fig. 4. *Top:* same as Fig. 3, but when the mass prediction is made using expressions from symbolic regression. Second and third panels show our two best results from Eqs. **11** and **14** (additional results are shown in *SI Appendix*, *Fig. S4*). Fourth panel compares the scatter in the mass residuals (the scatter is calculated using two different methods). We label the mass proxy in the second from *Top* panel as $Y_{\text{Conc.}}$. Introducting the term $(1-Ac_{\text{gas}})$ effectively down-weights the cluster cores in comparison to their outskirts (the cluster cores are relatively much noisier) and leads to a reduction in the scatter. *Bottom:* similar to the top case except the Y-M power-law slope is allowed to vary. Using $Y_{\text{Conc.}}$ reduces the scatter by $\sim 25\%$ for $M_{200c} \sim 2 \times 10^{14} M_{\odot}/h$.

We also obtained the following mass proxy which has an even better performance than Eq. 11:

$$M \propto Y_{200c}^{3/5} \left(\frac{B}{c_{
m NFW}}\right)^{M_*/M_{
m gas}},$$
 [14]

^{§§} Looking further into the future, CMB-HD could provide high-resolution observations of clusters (in case full cluster pressure profile information is available, other ML tools like deep sets can be used to obtain even more accurate mass predictions).

where B is another dimensionless constant (the best-fit value $B \sim 50$ is used in the figure). However, there are caveats regarding accurately estimating $M_*/M_{\rm gas}$ or $c_{\rm NFW}$ from observational data. Analogs of Y are typically estimated within $\lesssim 20\%$ in current CMB surveys (see, e.g., ref. 63). However, M_* can only be estimated to within a factor of $\gtrsim 50\%$ accuracy with the current galaxy surveys (see, e.g., refs. 66, 180–182). Therefore the mass estimation with Eq. 14 could be dominated by observational uncertainties. More importantly, estimating the NFW concentration ($c_{\rm NFW}$) requires high-resolution lensing observations and is therefore too expensive to measure for a large number of clusters. Therefore, we will use $Y_{\rm conc}$ from Eq. 11 as our main result for the rest of the paper.

In addition to using the lognormal assumption (Eq. 10) to calculate the scatter in Fig. 4, we nonparametrically calculate the scatter using quartiles of the mass residuals and find a similar improvement when our new equations are used. We leave testing the assumption of lognormality of the Y-M scatter to a future paper. Note also that we also obtained more complex equations as outputs from SR (some of them are shown in SIAppendix Fig. S4). However, given the large scatter already present in clusters from TNG300, the risk of overfitting goes up with increasing equation complexity. Hence, we show only the simplest expressions which have a relatively good performance.

In cluster cosmology analyses, the power-law index on Y-M is usually not fixed to 3/5, but is fitted to data. We therefore perform a test where we let the power-law index vary. We use the scipy.fit package and find the following best-fit relations: $M \propto Y^{0.59\pm0.002}$ and $M \propto Y^{0.618\pm0.002}(1-[0.61\pm0.02]c_{\rm gas})$. Their performance is shown in Fig. 4, Bottom.

Due to the lack of clusters in the high-mass end of the TNG300 simulation, we are unable to compare the scatter between the different models. Cosmological simulations with a larger number of high-mass clusters (e.g., MillleniumTNG) or hydrodynamical zoom-in simulations centered on massive halos of a dark matter only simulation e.g., the ones used in (152) would be valuable to test our results. Generally, we expect results from machine learning algorithms to improve with a larger training dataset.

C. Tests with CAMELS Simulations. Until this point, we showed results corresponding to the TNG300 simulation which uses a particular configuration of baryonic feedback parameters and a fixed cosmological model. However, the true nature of feedback in the Universe can be different, and we therefore want to test if the mass proxy $Y_{\rm conc}$ is robust to changes in feedback prescriptions. We therefore use the CAMELS suite of simulations which have varying cosmological and astrophysical feedback parameters, as well as varying initial conditions. We show our results for z=0 clusters in Fig. 5.

It is quite interesting that $Y_{\rm conc}$ consistently outperforms $Y_{\rm SZ}$ even when the feedback prescriptions in the simulations are very different. Note that we did not retrain the symbolic regressor using the CAMELS dataset, we merely used Eq. 11 and adjusted the constant A to optimize our results. We found that using a larger constant A'=0.8 for CAMELS-SIMBA works better than using A=0.4 which was obtained for TNG300 (for CAMELS-TNG, however, the same constant: A=0.4 gives optimal results). This difference could be related to the scatter in the cores of SIMBA clusters being larger; we will return to this point in section 5A. It is worth mentioning that the CAMELS simulations

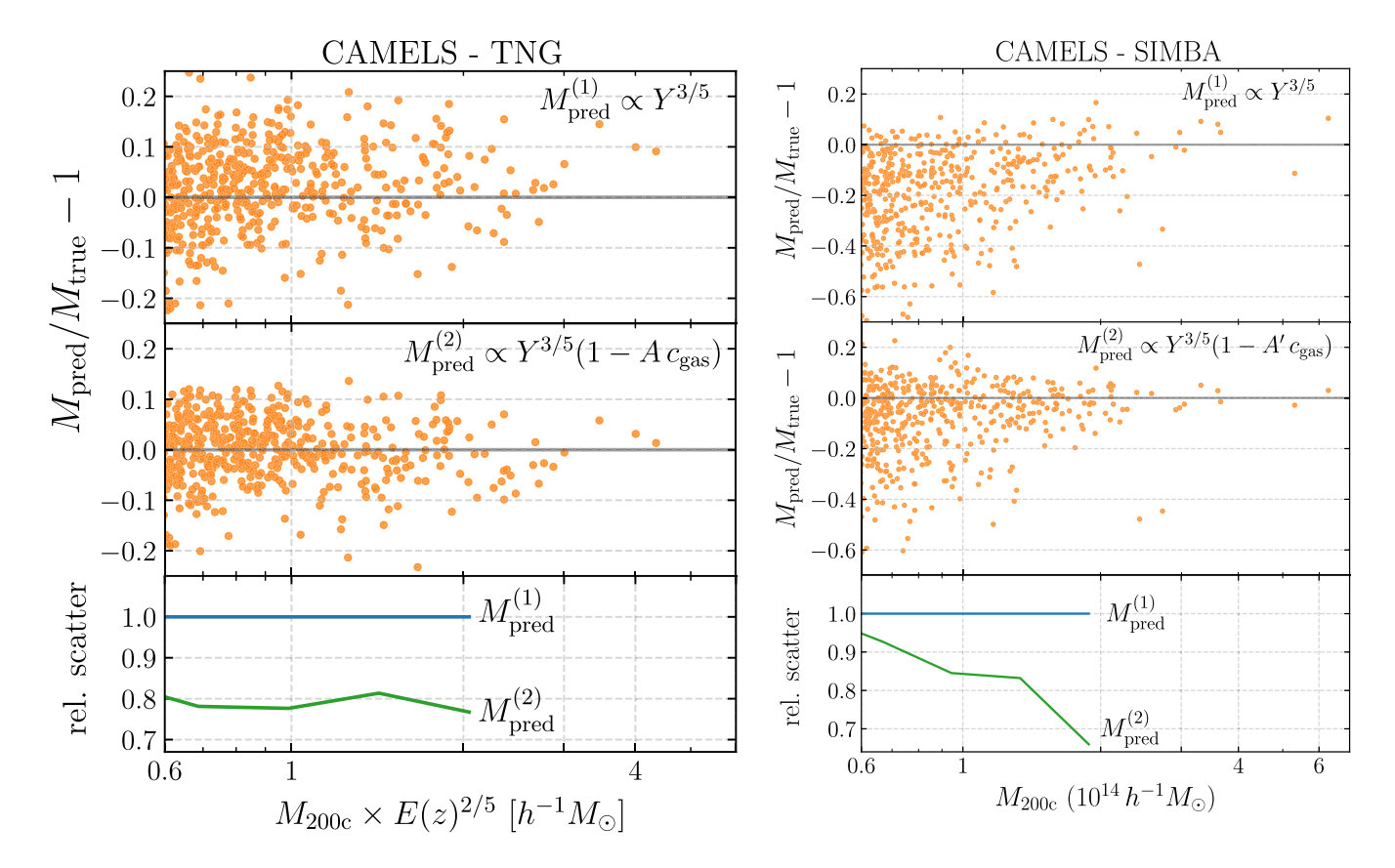


Fig. 5. Same as Fig. 4 but for halos in the CAMELS simulation suite instead of TNG300. As CAMELS includes variations in the baryonic feedback prescriptions in the hydrodynamic simulations, cosmological parameters and simulation initial seeds, the improvement upon using $M \propto Y_{\text{conc}}$ is robust against these changes. Note also for CAMELS-SIMBA that Y_{conc} not only reduces the scatter but also reduces the deviation from a power law for low M_{200c} .

have a small box size $(25 \ h^{-1} \ Mpc)$ and there are very few highmass clusters in the entire sample. It will be useful to check our results on the next iteration of the CAMELS simulations which will contain many more high-mass clusters.

5. Discussion

A. Dependence on Concentration. Having shown our results, let us now discuss some physical reasons behind the improvement in cluster mass prediction by taking into account concentration. For $A \in [0, 1]$, the term $(1-A\,c_{\rm gas})$ contributes toward effectively down-weighting the cluster cores in comparison to their outskirts. Downweighting/excising the central regions is desirable because observed cluster profiles show a greater degree of similarity outside the core (118, 121, 183, 184). To verify this, we show in Fig. 6 that the scatter in predicted mass is reduced when cluster cores are explicity excised from the calculation of Y_{200c} (Fig. 6 is for the TNG300 clusters, while the comparison with CAMELS clusters is shown in SI Appendix, Fig. S5).

Another way of verifying our results is to show the scatter in the pressure profile as a function of radius in the TNG300 clusters in Fig. 7 (see also Figure 4 of ref. 184 for comparison of pressure profile measurements from XMM-Newton and Planck). Note that the cores are the regions of clusters which are the most sensitive to nongravitational processes like radiative cooling and AGN feedback. Furthermore, simulations so far have not been able to convincingly reproduce the observed thermal structure of cool cores (see ref. 118), and the observed scatter in cluster cores could be larger than that predicted in simulations (121). Given that $Y_{\rm conc}$ at least partly corrects for the cluster core effects, we expect it to perform better in case the scatter in cluster cores is larger. We also expect our method to work better in case Y_{500c}

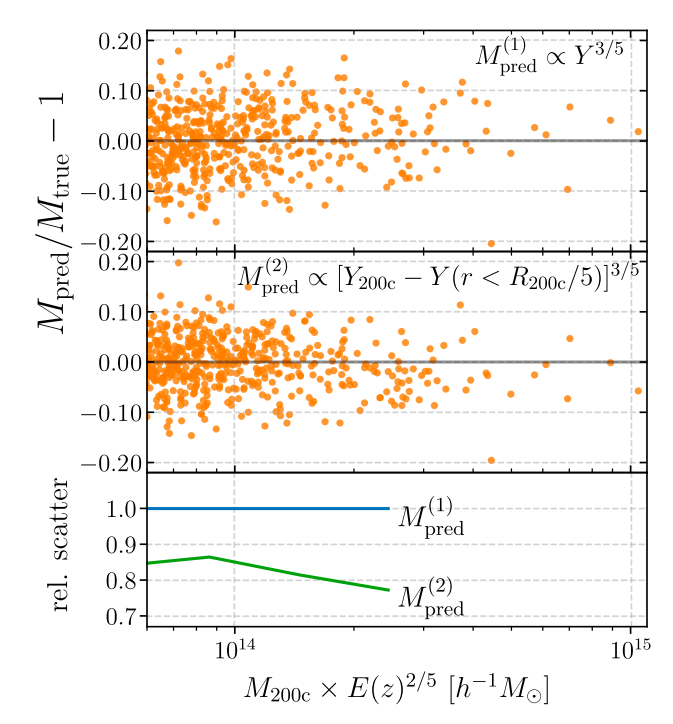


Fig. 6. Same as Fig. 4 but when the cores of the clusters are excised from the calculation of the integrated electron pressure. We see a roughly similar scatter reduction as in Fig. 4. Directly excising the cores in upcoming CMB surveys is difficult because of their low resolution, hence using Y_{conc} is beneficial.

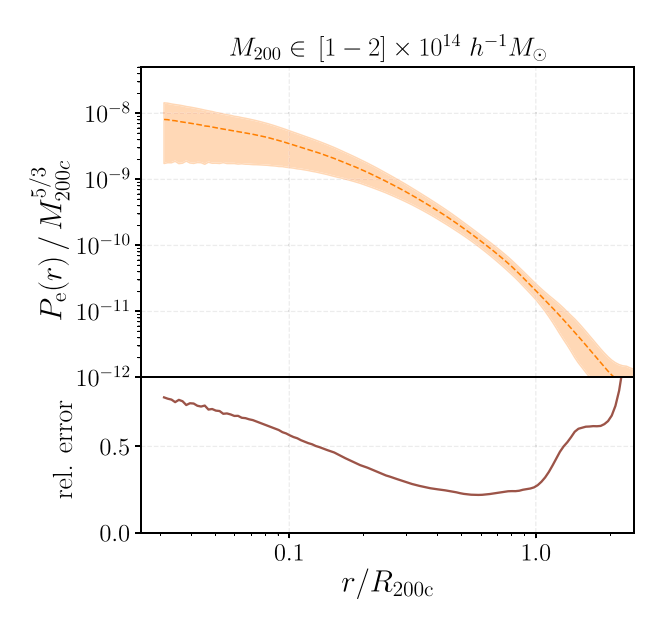


Fig. 7. Dependence of scatter with radius in the electron pressure profile (P_e) of clusters. We use the clusters from TNG300 in the specified mass range and show the mean and the 1σ region of the pressure profile scaled by the cluster mass. The profiles have a large scatter in the innermost regions (cores), while the outer regions (until R_{200c}) are relatively well-equilibrated.

is used instead of Y_{200c} as the contribution from cluster cores is relatively larger for Y_{500c} .

We explicitly show the dependence of Y-M relation on $c_{\rm gas}$, $c_{\rm NFW}$, and $M_*/M_{\rm gas}$ in Fig. 8, Top panel for halos in the mass range $10^{14} \le M \le 2 \times 10^{14} \ h^{-1} \ M_{\odot}$. The *Bottom* panel shows that $Y_{\rm conc}$ or Eq. 14 takes into account a major part of these dependencies (which is responsible for the improvement in the cluster mass prediction due to them).

B. Combining SZ and X-ray Observations. In the coming decade, numerous clusters will be probed with both X-ray, e.g., eROSITA survey (172, 185) and SZ surveys (e.g., SO). Let us now discuss ways in which these surveys can provide complementary information. The advantage of X-ray surveys over SZ surveys is their higher resolution. On the other hand, their disadvantage is that they probe the cluster thermal energy indirectly (assumptions about the gas density and temperature profiles are needed to estimate the integrated pressure in X-ray surveys, whereas it is directly measured in SZ surveys). Using $Y_{\rm conc}$ enables one to exploit this complementary behavior.

There are other advantages of combining SZ and X-ray surveys. Cross-calibration across different wavelength measurements generally helps in minimizing the possible systematics in individual measurements such as projection effects (see, e.g., ref. 186). Sometimes, $Y_{\rm spherical}$ reported by SZ surveys use an X-ray-derived estimate of the aperture size (as the cluster radii could be poorly measured by SZ surveys alone). X-ray and SZ surveys have different redshift dependence: The selection function of SZ surveys flattens toward higher redshifts, while X-ray surveys favor low-redshift systems. Combination of SZ and X-ray data can also help in removing outliers (e.g., recently merged clusters which deviate from the power-law relationship) and further tighten the *Y-M* relation (77).

C. Comparison with Previous Literature. Let us briefly mention some other proposals in the literature for augmenting the *Y-M* relation. Refs. (74, 75) proposed a fundamental plane relationship

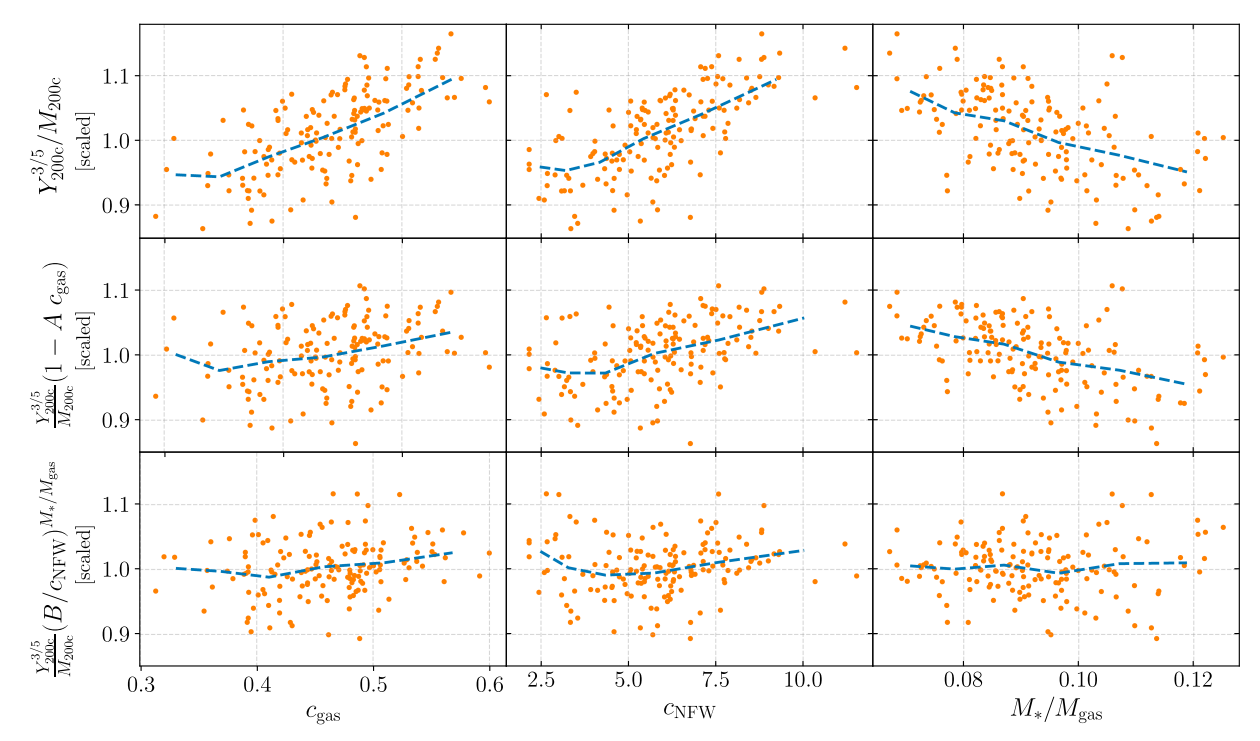


Fig. 8. Top panel: Dependence of the Y-M relation on gas concentration (c_{gas}), NFW concentration (c_{NFW}), and stellar to gas mass ratio (M_*/M_{gas}) for halos in the mass range $10^{14} \le M \le 2 \times 10^{14} \, h^{-1} \, M_{\odot}$. The dashed lines show the mean of the scatter. Higher c_{gas} (or c_{NFW}) is related to increase in the density of the ionized gas and can be a result of more radiative cooling (which in turn increases Y_{200c}). Higher M_*/M_{gas} implies more gas being converted into stars and is therefore associated with a decrease in Y_{200c} . Bottom panels: Using Y_{conc} (Middle) and Eq. **14** (Bottom) instead of Y_{200c} , for which the mean trends are comparatively weaker.

between Y, M, and the SZ half-light radius of the cluster. (187) proposed augmenting the thermal pressure profile of clusters with a model for the nonthermal pressure in order to ameliorate the hydrostatic mass bias effect. (76) noted that the NFW concentration can have an impact on the scatter in the Y-M relation. (77) proposed augmenting Y-M with a different form of cluster concentration: R_{200}/R_{500} . However, measuring this quantity requires high-resolution weak lensing data and this approach is therefore too expensive to be applied to a large number of clusters. Our analysis provides a way of augmenting the Y-M relation with properties that can be relatively easily measured in observational surveys. We also did a test with the random forest by adding analogs of the parameters proposed in the aforementioned studies for augmenting Y - M; we find that the RF predictions for cluster mass are improved only marginally (we show a comparison plot in SI Appendix, Fig. S6).

It is also worth mentioning that there have been studies augmenting other cluster scaling relations than *Y-M*, e.g., refs. 188, 189 and 190 proposed a fundamental plane between cluster temperature, its mass, and the scale radius of its matter profile. Recently, cluster NFW concentration was used in improving the model for the electron number density and pressure profiles of clusters (191).

6. Conclusions

Astrophysical scaling relations have a number of applications in inferring properties of stars, supernovae, black holes, galaxies, and clusters. With the upcoming high-precision astronomical surveys, it is imperative to find ways to augment the existing scaling relations in order to make them more accurate. Machine learning can provide a fast and systematic approach to search

for extensions to scaling relations in abstract high-dimensional parameter spaces.

We focused on searching for augmentations to the widely used $Y_{\rm SZ}-M$ scaling relation in order to make mass prediction of galaxy clusters more accurate. We first used a random forest regressor to search for a subset of parameters which give the most improvement in the cluster mass prediction (Fig. 3). We consequently used symbolic regression and found a new mass proxy which combines Y_{200c} and gas concentration ($c_{\rm gas}$): $M \propto Y_{\rm conc}^{3/5} \equiv Y_{200c}^{3/5} (1-A c_{\rm gas})$. $Y_{\rm conc}$ reduces the scatter in the mass prediction by $\sim 20-30\%$ for large clusters ($M_{200c} \gtrsim 10^{14} \, h^{-1} \, M_{\odot}$) at both high and low redshifts (Fig. 4). The new proxy exploits the complementary behavior of X-ray (high resolution but indirect probe of cluster thermal energy) and SZ (low resolution but direct probe of thermal energy) surveys.

We verified that $Y_{\rm conc}$ is robust against changes in both feedback parameters and subgrid physics by testing it with the CAMELS suite of simulations (Fig. 5). The dependence of $Y_{\rm conc}$ on $c_{\rm gas}$ is likely due to the cores of clusters being noisier (Fig. 7), and we verify this explicitly by excising the cores of clusters (Fig. 6). Our results and methodology can be useful for accurate multiwavelength cluster mass estimation from current and upcoming CMB and X-ray surveys like ACT, SO, eROSITA, and CMB-S4.

Future Work. We use three-dimensional cluster information (e.g., Y_{200c}) in this paper; but, in reality, projected properties of clusters (e.g., $Y_{cylindrical}$) are measured in surveys; we will try to test our results for that case in a future study. We focused on improving the Y-M relation for high M regime in this paper, but we use a similar ML-motivated methodology for improving Y-M in the low M regime in a more recent paper

(140). We could not robustly test $Y_{\rm conc}$ for very high mass clusters $(M \gtrsim 5 \times 10^{14} \, h^{-1} \, M_{\odot})$ due to lack of statistics, but we will do this test using clusters from the MilleniumTNG simulation (which has 15 times the volume of TNG300) in a separate upcoming paper.

As cluster observations improve, we will be able to use ML techniques directly on observed quantities and find the lowest scatter relations between lensing masses, microwave, and X-ray observables. Our methodology could also be useful for improving other widely used astrophysical scaling relations for exoplanets, stars, supernovae, galaxies, and clusters.

Data, Materials, and Software Availability. The code and data associated with this paper are available at https://github.com/JayWadekar/ScalingRelations_ML. All study data are included in the article and/or *SI Appendix*.

ACKNOWLEDGMENTS. First of all, we especially thank the anonymous referees for their critical comments as well as various useful suggestions on the manuscript. We also thank Daisuke Nagai, Nadia Zakamska, Matias Zaldarriaga,

- H. S. Leavitt, E. C. Pickering, Periods of 25 variable stars in the small magellanic cloud. Harvard Coll. Obser. Circ. 173, 1–3 (1912).
- A. G. Riess et al., A 2.4% determination of the local value of the Hubble constant. Astrophys. J. 826, 56 (2016).
- A. G. Riess, S. Casertano, W. Yuan, L. M. Macri, D. Scolnic, Large magellanic cloud cepheid standards provide a 1% foundation for the determination of the Hubble constant and stronger evidence for physics beyond ΛCDM. Astrophys. J. 876, 85 (2019).
- M. M. Phillips, The absolute magnitudes of type IA supernovae. Astrophys. J.I 413, L105 (1993)
- J. Kormendy, L. C. Ho, Coevolution (or not) of supermassive black holes and host galaxies. Annu. Rev. Astron. Astrophys. 51, 511-653 (2013).
- J. E. Greene, J. Strader, L. C. Ho, Intermediate-mass black holes. Annu. Rev. Astron. Astrophys. 58, 257–312 (2020).
- P. F. Hopkins, L. Hernquist, T. J. Cox, B. Robertson, E. Krause, An observed fundamental plane relation for supermassive black holes. *Astrophys. J.* 669, 67–73 (2007).
- R. B. Tully, J. R. Fisher, Reprint of 1977A&A.54.661T. A new method of determining distance to galaxies. Astron. Astrophys. 500, 105–117 (1977).
- S. S. McGaugh, J. M. Schombert, G. D. Bothun, W. J. G. de Blok, The baryonic Tully-Fisher relation. Astrophys. J. 533, 199-L102 (2000).
- S. M. Faber, R. E. Jackson, Velocity dispersions and mass-to-light ratios for elliptical galaxies. Astrophys. J. 204, 668–683 (1976).
- S. Djorgovski, M. Davis, Fundamental properties of elliptical galaxies. Astrophys. J. 313, 59 (1987).
- A. Dressler et al., Spectroscopy and photometry of elliptical galaxies I. New distance estimator.
- Astrophys. J. 313, 42 (1987).
 I. Jorgensen, M. Franx, P. Kjaergaard, The fundamental plane for cluster E and SO galaxies. Mon. Not. R. Astron. Soc. 280, 167–185 (1996).
- R. K. Sheth, M. Bernardi, Plain fundamentals of fundamental planes: Analytics and algorithms. Mon. Not. R. Astron. Soc. 422, 1825–1834 (2012).
- R. H. Wechsler, J. L. Tinker, The connection between galaxies and their dark matter halos. Annu. Rev. Astron. Astrophys. 56, 435-487 (2018).
- Planck Collaboration, P. A. R. Ade et al., Planck intermediate results. XI. The gas content of dark matter halos: The Sunyaev-Zeldovich-Stellar mass relation for locally brightest galaxies. Astron. Astrophys. 557, A52 (2013).
- A. V. Kravtsov, A. Vikhlinin, D. Nagai, A new robust low-scatter x-ray mass indicator for clusters of galaxies. Astrophys. J. 650, 128–136 (2006).
- N. Battaglia, J. R. Bond, C. Pfrommer, J. L. Sievers, On the cluster physics of Sunyaev-Zel'dovich and X-ray surveys. I. The influence of feedback, non-thermal pressure, and cluster shapes on Y-M scaling relations. Astrophys. J. 758, 74 (2012).
- A. Vikhlinin et al., Cosmological constraints from the evolution of the cluster Baryon Mass function at z 0.5. Astrophys. J. 590, 15-25 (2003).
- A. Voevodkin, A. Vikhlinin, Constraining amplitude and slope of the mass fluctuation spectrum using a cluster Baryon mass function. Astrophys. J. 601, 610-620 (2004).
- T. McClintock et al., Dark energy survey year 1 results: Weak lensing mass calibration of redMaPPer galaxy clusters. Mon. Not. R. Astron. Soc. 482, 1352–1378 (2019).
- 22. P. Langley, "Bacon: A production system that discovers empirical laws" in IJCAI (1977).
- M. Kokar, Determining arguments of invariant functional descriptions. Mach. Learn. 1, 403–422 (1986).
- P. Langley, J. M. Zytkow, Data-driven approaches to empirical discovery. Artif. Intell. 40, 283–312 (1989).
- R. Zembowicz, J. M. Żytkow, "Discovery of equations: Experimental evaluation of convergence" in Proceedings of the Tenth National Conference on Artificial Intelligence, AAAI 1992 (AAAI Press, 1992), pp. 70–75.
- J. Bongard, H. Lipson, From the cover: Automated reverse engineering of nonlinear dynamical systems. Proc. Natl. Acad. Sci. U.S.A. 104, 9943–9948 (2007).

Tibor Rothschild, Joshua Speagle, Niayesh Afshordi, Suzanne Staggs, and Abhishek Maniyar for fruitful discussions. D.W. gratefully acknowledges the support from the Friends of the Institute for Advanced Study Membership. F.V.-N. acknowledges funding from the WFIRST program through NNG26PJ30C and NNN12AA01C. N.B. acknowledges the support from NSF grant AST-1910021 and NASA grants 21-ADAP21-0114 and 21-ATP21-0129. D.A.A. was supported in part by NSF grants AST-2009687 and AST-2108944. The work of SH is supported by Center for Computational Astrophysics of the Flatiron Institute in New York City. The Flatiron Institute is supported by the Simons Foundation. JCH the acknowledges support from NSF grant AST-2108536. We also thank Boryana Hadzhiyska, Will Coulton, and Rachel Somerville for help with the ROCKSTAR catalogs corresponding to TNG halos.

Author affiliations: ^aSchool of Natural Sciences, Institute for Advanced Study, Princeton, NJ 08540; ^bCenter for Cosmology and Particle Physics, Department of Physics, New York University, New York, NY 10003; ^cDepartment of Physics, Princeton University, Princeton University, Princeton Strophysical Sciences, Princeton University, New York, NY 10010; ^cDepartment of Astrophysical Sciences, Princeton University, Princeton NJ 08544-0010; ^fDepartment of Physics, Columbia University, New York, NY 10027; ^gDepartment of Astronomy, Cornell University, Ithaca, NY 14853; ^hDepartment of Physics, University of Connecticut, Storrs, CT 06269; ^lCenter for Astrophysics | Harvard & Smithsonian, Cambridge, MA 02138; and ^jDepartment of Physics, Carnegie Mellon University, Pittsburgh, PA 15217

- M. Schmidt, H. Lipson, Distilling free-form natural laws from experimental data. Science 324, 81–85 (2009).
- S. Sahoo, C. Lampert, G. Martius, "Learning Equations for Extrapolation and Control" in *Proceedings of Machine Learning Research*, J. Dy, A. Krause, Eds., (PMLR, Stockholmsmässan, Stockholm Sweden, 2018), vol. 80, pp. 4442–4450.
- M. J. Kusner, B. Paige, J. M. Hernández-Lobato, Grammar Variational Autoencoder. arXiv [Preprint] (2017). https://arxiv.org/abs/1703.01925 (Accessed 2 March 2023).
- S. L. Brunton, J. L. Proctor, J. N. Kutz, Discovering governing equations from data by sparse identification of nonlinear dynamical systems. Proc. Natl. Acad. Sci. U.S.A. 113, 3932–3937 (2016).
- B. Lusch, J. N. Kutz, S. L. Brunton, Deep learning for universal linear embeddings of nonlinear dynamics. *Nat. Commun.* 9, 4950 (2018).
- H. Lange, S. L. Brunton, N. Kutz, From Fourier to Koopman: Spectral methods for long-term time series prediction. arXiv [Preprint] (2020). http://arxiv.org/abs/2004.00574 (Accessed 2 March 2023).
- G. J. Both, S. Choudhury, P. Sens, R. Kusters, DeepMoD: Deep learning for model discovery in noisy data. J. Comput. Phys. 428, 109985 (2021).
- C. Rackauckas et al., Universal differential equations for scientific machine learning. arXiv [Preprint] (2020). http://arxiv.org/abs/2001.04385 (Accessed 2 March 2023).
- R. Guimerà et al., A Bayesian machine scientist to aid in the solution of challenging scientific problems. Sci. Adv. 6, eaav6971 (2020).
- M. Virgolin, T. Alderliesten, C. Witteveen, P. A. N. Bosman, Improving model-based genetic programming for symbolic regression of small expressions. Evol. Comput. 29, 211–237 (2021).
- S. L. Brunton, J. L. Proctor, J. N. Kutz, Discovering governing equations from data by sparse identification of nonlinear dynamical systems. *Proc. Natl. Acad. Sci. U.S.A.* 113, 3932–3937 (2016).
- K. Champion, B. Lusch, J. N. Kutz, S. L. Srunton, Data-driven discovery of coordinates and governing equations. arXiv [Preprint] (2019). http://arxiv.org/abs/1904.02107 (Accessed 2 March 2023).
- M. Cranmer, et al., Discovering symbolic models from deep learning with inductive biases. NeurlPS. arXiv [Preprint] (2020). http://arxiv.org/abs/2006.11287 (Accessed 2 March 2023).
- M. Cranmer, Pysr: Fast & parallelized symbolic regression in Python/Julia Version 0.11.9 (2020). https://libraries.io/conda/pysr (Accessed 2 March 2023).
- M. D. Cranmer, R. Xu, P. Battaglia, S. Ho, Learning symbolic physics with graph networks. NeurIPS Workshop on Physics and Machine Learning. arXiv [Preprint] (2019). http://arxiv.org/abs/1909. 05862 (Accessed 2 March 2023).
- M. Vastl, J. Kulhánek, J. Kubalík, E. Derner, R. Babuška, SymFormer: End-to-end symbolic regression using transformer-based architecture. arXiv [Preprint] (2022). http://arxiv.org/abs/ 2205.15764 (Accessed 2 March 2023).
- A. M. Delgado et al., Modeling the galaxy-halo connection with machine learning. Mon. Notices Royal Astron. Soc. 515, 2733–2746 (2022).
- D. Wadekar, F. Villaescusa-Navarro, S. Ho, L. Perreault-Levasseur, Modeling assembly bias with machine learning and symbolic regression. arXiv [Preprint] (2020). http://arxiv.org/abs/2012. 00111 (Accessed 2 March 2023).
- M. J. Graham, S. G. Djorgovski, A. A. Mahabal, C. Donalek, A. J. Drake, Machine-assisted discovery of relationships in astronomy. *Mon. Not. R. Astron. Soc.* 431, 2371–2384 (2013).
- of relationships in astronomy. *Mon. Not. R. Astron. Soc.* **431**, 2371–2384 (2013).

 46. M. J. Graham *et al.*, Data challenges of time domain astronomy. arXiv [Preprint] (2012). http://arxiv.org/abs/1208.2480 (Accessed 2 March 2023).
- H. Shao et al., Finding universal relations in subhalo properties with artificial intelligence. Astrophys. 927, 85 (2022).
- Z. Liu, M. Tegmark, Al Poincaré: Machine learning conservation laws from trajectories. arXiv [Preprint] (2020). http://arxiv.org/abs/2011.04698 (Accessed 2 March 2023).
 C. Wilstrup, J. Kasak, Symbolic regression outperforms other models for small data sets. arXiv
- [Preprint] (2021). http://arxiv.org/abs/2103.15147 (Accessed 2 March 2023).

 50. P. Lemos, N. Jeffrey, M. Cranmer, P. Battaglia, S. Ho, Rediscovering Newton's gravity and solar
- system properties using deep learning and inductive biases (2022).
 51. A. Butter, T. Plehn, N. Soybelman, J. Brehmer, *Back to the Formula LHC Edition* (2021).
- 52. W. Gilpin, Chaos as an interpretable benchmark for forecasting and data-driven modelling (2021).

- M. Cranmer et al., "Disentangled sparsity networks for explainable AI" in Workshop on Sparse Neural Networks (2021), p. 7.
- M. Cranmer et al., "Histogram pooling operators: An interpretable alternative for deep sets" in ICLR 2021 SimDL Workshop (2021), p. 10.
- J. Craven, V. Jejjala, A. Kar, Disentangling a deep learned volume formula. J. High Energ. Phys.
- 56. M. Werner, A. Junginger, P. Hennig, G. Martius, Informed equation learning. arXiv [Preprint] (2021) https://arxiv.org/abs/2105.06331 (Accessed 2 March 2023).
- A. Krone-Martins, E. E. O. Ishida, R. S. de Souza, The first analytical expression to estimate 57. photometric redshifts suggested by a machine. Mon. Not. R. Astron. Soc. 443, L34-L38 (2014).
- J. L. Bernal, A. Caputo, F. Villaescusa-Navarro, M. Kamionkowski, Searching for the radiative 58. decay of the cosmic neutrino background with line-intensity mapping. Phys. Rev. Lett. 127, 131102 (2021).
- F. Villaescusa-Navarro et al., The CAMELS project: Cosmology and astrophysics with machine-59.
- learning simulations. *Astrophys. J.* **915**, 71 (2021).
 P. A. R. Ade *et al.*, Planck 2015 results. XXIV. Cosmology from Sunyaev-Zeldovich cluster counts. *Astron. Astrophys.* **594**, A24 (2016).
- P. A. R. Ade et al., Planck 2015 results. XXVII. The second planck catalogue of Sunyaev-Zeldovich sources. Astron. Astrophys. 594, A27 (2016).
- M. Hasselfield et al., The atacama cosmology telescope: Sunyaev-Zel'dovich selected galaxy clusters at 148 GHz from three seasons of data. J. Cosmol. Astropart. Phys. 2013, 008 (2013).
- M. Hilton et al., The atacama cosmology telescope: A catalog of >4000 Sunyaev-Zel'dovich Galaxy Clusters. Astrophys. J. 253, 3 (2021).
- S. Bocquet et al., Mass calibration and cosmological analysis of the SPT-SZ galaxy cluster sample using velocity dispersion α_V and x-ray Y_X measurements. Astrophys. J. **799**, 214 (2015).
- S. Bocquet et al., Cluster cosmology constraints from the 2500 deg² spt-sz survey: Inclusion of weak gravitational lensing data from magellan and the hubble space telescope. Astrophys. J. **878**, 55 (2019).
- A. Palmese et al., Stellar mass as a galaxy cluster mass proxy: Application to the dark energy survey redmapper clusters. Mon. Not. R. Astron. Soc. 493, 4591-4606 (2020).
- S.W. Allen, A. E. Evrard, A. B. Mantz, Cosmological parameters from observations of galaxy clusters. *Annu. Rev. Astron. Astrophys.* **49**, 409–470 (2011).

 N. Sehgal *et al.*, The atacama cosmology telescope: Cosmology from galaxy clusters detected via
- the Sunyaev-Zel'dovich effect. *Astrophys. J.* **732**, 44 (2011).

 Planck Collaboration *et al.*, Planck 2015 results. XXIV. Cosmology from Sunyaev-Zeldovich cluster
- counts. Astron. Astrophys. 594, A24 (2016).
- S. Bocquet et al., Cluster Cosmology Constraints from the 2500 deg² SPT-SZ survey: Inclusion of weak gravitational lensing data from magellan and the Hubble space telescope. Astrophys. J. 878, 55 (2019).
- M. S. Madhavacheril, N. Battaglia, H. Miyatake, Fundamental physics from future weak-lensing calibrated Sunyaev-Zel'dovich galaxy cluster counts. Phys. Rev. D 96, 103525 (2017).
- S. Mishra-Sharma, D. Alonso, J. Dunkley, Neutrino masses and beyond- A CDM cosmology with LSST and future CMB experiments. Phys. Rev. D 97, 123544 (2018).
- L. D. Shaw, G. P. Holder, J. Dudley, Non-Gaussian scatter in cluster scaling relations. Astrophys. J. 716, 281-285 (2010).
- L. Verde, Z. Haiman, D. N. Spergel, Are clusters standard candles? Galaxy cluster scaling relations with the Sunyaev-Zeldovich effect. Astrophys. J. **581**, 5–19 (2002).
- N. Afshordi, Fundamental plane of Sunyaev-Zel'dovich clusters. *Astrophys. J.* **686**, 201–205 (2008)
- L. D. Shaw, G. P. Holder, P. Bode, The impact of halo properties, energy feedback, and projection effects on the mass-SZ flux relation. *Astrophys. J.* **686**, 206–218 (2008). H. Y. K. Yang, S. Bhattacharya, P. M. Ricker, The impact of cluster structure and dynamical state on
- scatter in the Sunyaev-Zel'dovich flux-mass relation. Astrophys. J. 725, 1124-1136 (2010).
- S. B. Green et al., Using X-ray morphological parameters to strengthen galaxy cluster mass estimates via machine learning. Astrophys. J. 884, 33 (2019).
- J. D. Cohn, N. Battaglia, Multiwavelength cluster mass estimates and machine learning. Mon. Not. R. Astron. Soc. 491, 1575-1584 (2020).
- M. Ntampaka et al., A machine learning approach for dynamical mass measurements of galaxy clusters. Astrophys. J. 803, 50 (2015).
- M. Ntampaka et al., The role of machine learning in the next decade of cosmology (2019).
- M. Ho et al., A robust and efficient deep learning method for dynamical mass measurements of galaxy clusters. Astrophys. J. 887, 25 (2019).
- D. Kodi Ramanah, R. Wojtak, Z. Ansari, C. Gall, J. Hjorth, Dynamical mass inference of galaxy clusters with neural flows. Mon. Not. R. Astron. Soc. 499, 1985-1997 (2020).
- D. Kodi Ramanah, R. Wojtak, N. Arendse, Simulation-based inference of dynamical galaxy cluster masses with 3D convolutional neural networks. Mon. Not. R. Astron. Soc. 501, 4080-4091 (2021).
- 85 N. Gupta, C. L. Reichardt, Mass estimation of galaxy clusters with deep learning I. Sunyaev-
- N. Cupta, C. L. Reichardt, Mass estimation of galaxy clusters with deep learning I. Sunyaev Zel'dovich effect. *Astrophys. J.* **900**, 110 (2020).

 N. Gupta, C. L. Reichardt, Mass estimation of galaxy clusters with deep learning II: Cosmic Microwave Background cluster lensing. *Astrophys.* **923**, 96 (2021).
- Y. Su et al., A deep learning view of the census of galaxy clusters in illustristng. Mon. Not. R. Astron. Soc. 498, 5620-5628 (2020).
- Z. Yan, A. J. Mead, L. Van Waerbeke, G. Hinshaw, I. G. McCarthy, Galaxy cluster mass estimation with deep learning and hydrodynamical simulations. Mon. Not. R. Astron. Soc. 499, 3445-3458 (2020).
- P. Villanueva-Domingo et al., Inferring halo masses with graph neural networks. Astrophys. 935, 30 (2022).
- M. Ntampaka, A. Vikhlinin, The importance of being interpretable: Toward an understandable machine learning encoder for galaxy cluster cosmology. *Astrophys. J.* **926**, 45 (2022). T. J. Armitage, S. T. Kay, D. J. Barnes, An application of machine learning techniques to galaxy
- cluster mass estimation using the MACSIS simulations. Mon. Not. R. Astron. Soc. 484, 1526-
- A. Ferragamo et al., The three hundred project: A machine learning method to infer clusters of galaxies mass radial profiles from mock Sunyaev-Zel'dovich maps. arXiv [Preprint] (2022). http://arxiv.org/abs/2207.12337 (Accessed 2 March 2023).

- D. de Andres et al., A deep learning approach to infer galaxy cluster masses from Planck Compton-y parameter maps. Nat. Astron. 6, 1325-1331 (2022).
- D. Nelson et al., The illustristing simulations: Public data release. Comput. Astrophys. Cosmol. 6, 2
- A. Pillepich et al., First results from the illustristng simulations: The stellar mass content of groups and clusters of galaxies. Mon. Not. R. Astron. Soc. 475, 648-675 (2018).
- V. Springel et al., First results from the IllustrisTNG simulations: Matter and galaxy clustering. Mon. Not. R. Astron. Soc. 475, 676-698 (2018).
- D. Nelson et al., First results from the IllustrisTNG simulations: The galaxy colour bimodality. Mon. Not. R. Astron. Soc. 475, 624-647 (2018).
- J. P. Naiman et al., First results from the illustristing simulations: A tale of two elements chemical evolution of magnesium and europium. Mon. Not. R. Astron. Soc. 477, 1206–1224 (2018).
- F. Marinacci et al., First results from the illustristing simulations: Radio haloes and magnetic fields. Mon. Not. R. Astron. Soc. 480, 5113-5139 (2018).
- A. Pillepich et al., Simulating galaxy formation with the IllustrisTNG model. Mon. Not. R. Astron. Soc. 473, 4077-4106 (2018).
- R. Weinberger et al., Simulating galaxy formation with black hole driven thermal and kinetic feedback. Mon. Not. R. Astron. Soc. 465, 3291-3308 (2017).
- V. Springel, E pur si muove: Galilean-invariant cosmological hydrodynamical simulations on a moving mesh. Mon. Not. R. Astron. Soc. 401, 791-851 (2010).
- R. Weinberger, V. Springel, R. Pakmor, The AREPO public code release. Astrophys. J.s 248, 32
- F. Villaescusa-Navarro et al., The CAMELS multifield dataset: Learning the universe's fundamental parameters with artificial intelligence. arXiv [Preprint] (2021). http://arxiv.org/abs/2109.10915 (Accessed 2 March 2023).
- P. F. Hopkins, A new class of accurate, mesh-free hydrodynamic simulation methods. Mon. Not. R. Astron. Soc. 450, 53-110 (2015).
- P. F. Hopkins, A new public release of the GIZMO code. arXiv [Preprint] (2017). http://arxiv.org/ abs/1712.01294 (Accessed 2 March 2023).
- R. Davé et al., SIMBA: Cosmological simulations with black hole growth and feedback. Mon. Not. R. Astron. Soc. 486, 2827-2849 (2019).
- R. Weinberger et al., Supermassive black holes and their feedback effects in the IllustrisTNG simulation. Mon. Not. R. Astron. Soc. 479, 4056-4072 (2018).
- D. Anglés-Alcázar, R. Davé, C. A. Faucher-Giguère, F. Özel, P. F. Hopkins, Gravitational torquedriven black hole growth and feedback in cosmological simulations. Mon. Not. R. Astron. Soc. 464, 2840-2853 (2017).
- 110. B. Everitt, S. Landau, M. Leese, D. Stahl, Safari aORMC Cluster Analysis (John Wiley & Sons, ed. 5, 2011).
- J. Tinker et al., Toward a halo mass function for precision cosmology: The limits of universality. Astrophys. J. 688, 709-728 (2008).
- R. A. Sunyaev, Y. B. Zeldovich, Small-scale fluctuations of relic radiation. Astrophys. Space Sci. 7, 3-19 (1970).
- J. H. Croston, M. Arnaud, E. Pointecouteau, G. W. Pratt, An improved deprojection and PSF deconvolution technique for galaxy-cluster X-ray surface-brightness profiles. Astron. Astrophys. **459**, 1007-1019 (2006).
- A. A. Klypin, S. Trujillo-Gomez, J. Primack, Dark matter halos in the standard cosmological model: Results from the Bolshoi Simulation. Astrophys. J. 740, 102 (2011).
- A. Gabrielpillai et al., Galaxy formation in the Santa Cruz semi-analytic model compared with IllustrisTNG - I. Galaxy scaling relations, dispersions, and residuals at z=0. Mon. Notices Royal Astron. Soc. 517, 6091-6111 (2022).
- P. S. Behroozi, R. H. Wechsler, H. Y. Wu, The rockstar phase-space temporal halo finder and the velocity offsets of cluster cores. Astrophys. J. 762, 109 (2013).
- N. Kaiser, Evolution and clustering of rich clusters. Mon. Not. R. Astron. Soc. 222, 323–345 (1986).
- 118. A. V. Kravtsov, S. Borgani, Formation of galaxy clusters. Annu. Rev. Astron. Astrophys. 50, 353-409 (2012).
- G. L. Bryan, M. L. Norman, Statistical properties of x-ray clusters: Analytic and numerical comparisons. Astrophys. J. 495, 80-99 (1998).
- R. Stanek, E. Rasia, A. E. Evrard, F. Pearce, L. Gazzola, Massive halos in millennium gas simulations: multivariate scaling relations. Astrophys. J. 715, 1508-1523 (2010).
- M. Arnaud et al., The universal galaxy cluster pressure profile from a representative sample of nearby systems (REXCESS) and the Y_{SZ} - M₅₀₀ relation. Astron. Astrophys. 517, A92 (2010).
- D. Fabjan et al., X-ray mass proxies from hydrodynamic simulations of galaxy clusters I. Mon. Not. R. Astron. Soc. 416, 801-816 (2011).
- W. Hu, S. DeDeo, C. Vale, Cluster mass estimators from CMB temperature and polarization lensing. New J. Phys. 9, 441 (2007).
- E. J. Baxter et al., A measurement of gravitational lensing of the cosmic microwave background by galaxy clusters using data from the south pole telescope. *Astrophys. J.* **806**, 247 (2015).
- J. E. Geach, J. A. Peacock, Cluster richness-mass calibration with cosmic microwave background lensing. Nat. Astron. 1, 795-799 (2017).
- M. S. Madhavacheril et al., The atacama cosmology telescope: Weighing distant clusters with the most ancient light. Astrophys. J.I 903, L13 (2020).
- H. Hoekstra et al., Masses of galaxy clusters from gravitational lensing. Space Sci. Rev. 177 (1-4),
- A. von der Linden et al., Robust weak-lensing mass calibration of Planck galaxy clusters. Mon. Not. R. Astron. Soc. 443, 1973-1978 (2014).
- N. Battaglia et al., Weak-lensing mass calibration of the atacama cosmology telescope equatorial Sunyaev-Zeldovich cluster sample with the Canada-France-Hawaii telescope stripe 82 survey. J. Cosmol. Astropart. Phys. 2016, 013 (2016).
- E. Medezinski et al., Planck Sunyaev-Zel'dovich cluster mass calibration using hyper Suprime-Cam weak lensing. Publ. Astron. Soc. Jpn. 70, S28 (2018).
- T. Schrabback et al., Cluster mass calibration at high redshift: HST weak lensing analysis of 13 distant galaxy clusters from the south pole telescope Sunyaev-Zel'dovich survey. Mon. Not. R. Astron. Soc. 474, 2635-2678 (2018).

- 132. H. Miyatake et al., Weak-lensing mass calibration of actpol Sunyaev-Zeldovich clusters with the hyper suprime-cam survey. Astrophys. J. 875, 63 (2019).
- S. Majumdar, J. J. Mohr, Importance of cluster structural evolution in using x-ray and Sunyaev-Zeldovich effect galaxy cluster surveys to study dark energy. Astrophys. J. 585, 603-610 (2003).
- S. Majumdar, J. J. Mohr, Self-calibration in cluster studies of dark energy: Combining the cluster redshift distribution, the power spectrum, and mass measurements. Astrophys. J. 613, 41-50
- 135. M. R. Lovell et al., The fraction of dark matter within galaxies from the IllustrisTNG simulations. Mon. Not. R. Astron. Soc. 481, 1950-1975 (2018).
- J. C. Hill, E. J. Baxter, A. Lidz, J. P. Greco, B. Jain, Two-halo term in stacked thermal Sunyaev-136.
- Zel'dovich measurements: Implications for self-similarity. *Phys. Rev. D* **97**, 083501 (2018).

 A. M. C. Le Brun, I. G. McCarthy, J. B. Melin, Testing Sunyaev-Zel'dovich measurements of the hot gas content of dark matter haloes using synthetic skies. *Mon. Not. R. Astron. Soc.* **451**, 3868–383 3881 (2015).
- J. P. Greco, J. C. Hill, D. N. Spergel, N. Battaglia, The stacked thermal Sunyaev-Zel'dovich signal of 138. locally brightest galaxies in Planck full mission data: evidence for galaxy feedback? Astrophys. J. 808, 151 (2015).
- S. Pandey et al., Cross-correlation of DES Y3 lensing and ACT/Planck thermal Sunyaev Zel'dovich Effect II: Modeling and constraints on halo pressure profiles. Phys. Rev. D. 105, 123526 (2022).
- D. Wadekar et al., The SZ flux-mass (Y-M) relation at low halo masses: Improvements with symbolic regression and strong constraints on baryonic feedback. arXiv [Preprint] (2022). http://arxiv.org/abs/2209.02075 (Accessed 2 March 2023).
- S. He et al., Learning to predict the cosmological structure formation. Proc. Natl. Acad. Sci. U.S.A. 116, 13825-13832 (2019).
- D. Wadekar, F. Villaescusa-Navarro, S. Ho, L. Perreault-Levasseur, Hlnet: Generating neutral hydrogen from dark matter with neural networks. Astrophys. J. 916, 42 (2021).
- X. Zhang et al., From dark matter to galaxies with convolutional networks. arXiv [Preprint] (2019). http://arxiv.org/abs/1902.05965 (Accessed 2 March 2023).
- E. Giusarma et al., Learning neutrino effects in cosmology with convolutional neural networks. arXiv [Preprint] (2019). http://arxiv.org/abs/1910.04255 (Accessed 2 March 2023).
- C. D. Kreisch et al., The GIGANTES dataset: Precision cosmology from voids in the machine learning era. Astrophys. 935, 100 (2022).
- 146. J. H. T. Yip et al., From dark matter to galaxies with convolutional neural networks. arXiv [Preprint] (2019). http://arxiv.org/abs/1910.07813 (Accessed 2 March 2023).
- N. Kaushal et al., NECOLA: Towards a universal field-level cosmological emulator. Astrophys. 930, 115 (2022).
- J. Zamudio-Fernandez et al., HIGAN: cosmic neutral hydrogen with generative adversarial networks. arXiv [Preprint] (2019). http://arxiv.org/abs/1904.12846 (Accessed 2 March 2023).
- C. Modi, Y. Feng, U. Seljak, Cosmological reconstruction from galaxy light: Neural network based light-matter connection. J. Cosmol. Astropart. Phys. 2018, 028 (2018).
- D. Kodi Ramanah, T. Charnock, F. Villaescusa-Navarro, B. D. Wandelt, Super-resolution emulator of cosmological simulations using deep physical models. Mon. Not. R. Astron. Soc. 495, 4227-
- 151. T. Tröster, C. Ferguson, J. Harnois-Déraps, I. G. McCarthy, Painting with baryons: Augmenting Nbody simulations with gas using deep generative models. Mon. Not. R. Astron. Soc. 487, L24-L29 $(20\dot{1}9).$
- L. Thiele, F. Villaescusa-Navarro, D. N. Spergel, D. Nelson, A. Pillepich, Teaching neural networks
- to generate Fast Sunyaev Zel'dovich maps. *Astrophys.* **902**, 129 (2020). 153. M. Cranmer *et al.*, Discovering symbolic models from deep learning with inductive biases (2020). 154. L. Thiele, M. Cranmer, W. Coulton, S. Ho, D. N. Spergel, "Equivariant and modular DeepSets
- with applications in cluster cosmology" in NeurIPS Workshop on Physics and Machine Learning
- P. Berger, G. Stein, A volumetric deep convolutional neural network for simulation of mock dark matter halo catalogues. Mon. Not. R. Astron. Soc. 482, 2861-2871 (2019).
- B. Horowitz, M. Dornfest, Z. Lukić, P. Harrington, HyPhy: Deep generative conditional posterior mapping of hydrodynamical physics. Astrophys 941, 42 (2022).
- F. Villaescusa-Navarro et al., Multifield Cosmology with Artificial Intelligence. arXiv [Preprint] (2021). http://arxiv.org/abs/2109.09747 (Accessed 2 March 2023).
- F. Villaescusa-Navarro et al., Robust marginalization of baryonic effects for cosmological inference at the field level. arXiv [Preprint] (2021). http://arxiv.org/abs/2109.10360 (Accessed 2 March
- 159. T. Lu, Z. Haiman, J. M. Zorrilla Matilla, Simultaneously constraining cosmology and baryonic physics via deep learning from weak lensing. Mon. Notices Royal Astron. Soc. 511, 1518-1528 (2022).
- Y. Li et al., Al-assisted superresolution cosmological simulations. Proc. Natl. Acad. Sci. U.S.A. 118, 2022038118 (2021).

- Y. Ni et al., Al-assisted super-resolution cosmological simulations II: Halo substructures, velocities and higher order statistics. Mon. Notices Royal Astron. Soc. 507, 1021-1033 (2021).
- L. Breiman, Random forests. Mach. Learn. 45, 5-32 (2001).
- J. Elith, J. R. Leathwick, T. Hastie, A working guide to boosted regression trees. J. Anim. Ecol. 77, 802-813 (2008).
- A. A. Miller et al., A machine-learning method to infer fundamental stellar parameters from photometric light curves. Astrophys. J. 798, 122 (2015).
- D. Valencia, E. Paracha, A. P. Jackson, Can a machine learn the outcome of planetary collisions? Astrophys. J. 882, 35 (2019).
- S. Agarwal, R. Davé, B. A. Bassett, Painting galaxies into dark matter haloes using machine learning. Mon. Not. R. Astron. Soc. 478, 3410-3422 (2018).
- L. Lucie-Smith, H. V. Peiris, A. Pontzen, M. Lochner, Machine learning cosmological structure formation. Mon. Not. R. Astron. Soc. 479, 3405-3414 (2018).
- B. P. Moster, T. Naab, M. Lindström, J. A. O'Leary, GalaxyNet: Connecting galaxies and dark matter haloes with deep neural networks and reinforcement learning in large volumes. Mon. Notices Royal Astron. Soc. 507, 2115-2136 (2021).
- E. O. Nadler, Y. Y. Mao, R. H. Wechsler, S. Garrison-Kimmel, A. Wetzel, Modeling the impact of baryons on subhalo populations with machine learning. Astrophys. J. 859, 129 (2018).
- S. Mucesh et al., A machine learning approach to galaxy properties: Joint redshift stellar mass probability distributions with random forest. Mon. Notices Royal Astron. Soc. 502, 2770-2786 (2020)
- Q. Li et al., What to expect from dynamical modelling of cluster haloes II. Investigating dynamical state indicators with random forest. Mon. Not. R. Astron. Soc. 514, 5890-5904
- A. Liu et al., The eROSITA final equatorial-depth survey (eFEDS). Catalog of galaxy clusters and groups. Astron. Astrophys. 661, A2 (2022).
- F. Pedregosa et al., Scikit-learn: Machine learning in python. J. Mach. Learn. Res. 12, 2825-2830
- M. Kutner, Applied Linear Statistical Models, McGrwa-Hill International Edition (McGraw-Hill Irwin, 2005).
- S. Sheather, A Modern Approach to Regression with R, Springer Texts in Statistics (Springer, New York, NY, 2009).
- J. Fox, S. Weisberg, An R Companion to Applied Regression (SAGE Publications, 2011).
- L. Kawinwanichakij et al., Effect of local environment and stellar mass on galaxy quenching and morphology at 0.5 z 2.0. Astrophys. J. 847, 134 (2017).
- V. F. Braga et al., On the RR Lyrae Stars in Globulars. V. The complete near-infrared (JHK s) Census of ω centauri RR lyrae variables. Astron. J. **155**, 137 (2018).
- H. Li et al., Interpreting the star formation-extinction relation with MaNGA. Astrophys. J. 872, 63 (2019).
- S. Huang $\it{et\,al.}$, Individual stellar haloes of massive galaxies measured to 100 kpc at 0.3 z 0.5 using Hyper Suprime-Cam. Mon. Not. R. Astron. Soc. 475, 3348-3368 (2018).
- S. Huang et al., Weak lensing reveals a tight connection between dark matter halo mass and the distribution of stellar mass in massive galaxies. Mon. Not. R. Astron. Soc. 492, 3685-3707
- C. Hahn et al., The desi probabilistic value-added bright galaxy survey (provabgs) mock challenge. arXiv [Preprint] (2022). http://arxiv.org/abs/2202.01809 (Accessed 2 March 2023).
- A. Vikhlinin et al., Chandra sample of nearby relaxed galaxy clusters: mass, gas fraction, and mass-temperature relation. Astrophys. J. 640, 691-709 (2006).
- Planck Collaboration et al., Planck intermediate results. V. Pressure profiles of galaxy clusters from the Sunyaev-Zeldovich effect. Astron. Astrophys. 550, A131 (2013).
- I. N. Chiu, M. Klein, J. Mohr, S. Bocquet, Cosmological constraints from galaxy clusters and groups in the *erosita* final equatorial depth survey. arXiv [Preprint] (2022). http://arxiv.org/abs/ 2207.12429 (Accessed 2 March 2023).
- F. Menanteau et al., The atacama cosmology telescope: physical properties and purity of a galaxy cluster sample selected via the sunyaev-zel'dovich effect. Astrophys. J. 723, 1523-1541 (2010).
- K. Nelson, D. H. Rudd, L. Shaw, D. Nagai, Evolution of the merger-induced hydrostatic mass bias in galaxy clusters. Astrophys. J. 751, 121 (2012).
- Y. Fujita et al., Discovery of a new fundamental plane dictating galaxy cluster evolution from gravitational lensing. Astrophys. J. 857, 118 (2018).
- Y. Fujita et al., A new interpretation of the mass-temperature relation and mass calibration of galaxy clusters based on the fundamental plane. Astrophys. J. 863, 37 (2018).
- Y. Fujita et al., Halo concentrations and the fundamental plane of galaxy clusters. Galaxies 7, 8 (2019).
- B. K. K. Lee, W. R. Coulton, L. Thiele, S. Ho, An exploration of the properties of cluster profiles for the thermal and kinetic Sunyaev-Zel'dovich effects. arXiv [Preprint] (2022). http://arxiv.org/abs/ 2205.01710 (Accessed 2 March 2023).